Investigating the Effect of Current Density on Electrodeposited Ni-TiC-WC Composite Coating and Evaluating the Corrosion Resistance of the Coating and Substrate in NaCl solution

A. Keramatian[a], M.H. Enayati[a], F.S. Sayyedan[b,*], S. Torkian[a]

[a] Department of Materials Engineering, Isfahan University of Technology, Isfahan 8415683111, Iran

[b] Department of Materials Science and Engineering, Faculty of Engineering, Ferdowsi University of Mashhad, Mashhad 9177948944, Iran

Abstract

The aim of this study was to investigate the effect of current density on the microstructure of electrodeposited Ni–WC–TiC composite coatings on 304 stainless steel and compare the corrosion resistance of the coating and substrate in a 3.5 wt.% sodium chloride solution. A Watts nickel bath was employed under direct current (DC) conditions. Microstructure, elemental composition, and phase composition analyses were conducted using scanning electron microscopy (SEM) equipped with energy-dispersive X-ray spectroscopy (EDS) and X-ray diffraction (XRD), respectively. The results revealed that the coating formed at a current density of 40 mA/cm² exhibited a denser microstructure with higher cohesion and uniformity compared to coatings produced at other current densities. The corrosion resistance of the coating and substrate was evaluated using Tafel and electrochemical impedance spectroscopy (EIS) analyses. The corrosion test results indicated that the substrate exhibited superior corrosion resistance compared to the coating. Based on the dynamic polarization test plots, the corrosion mechanism of the substrate is active-quasi passive, with a pseudo-passive layer forming on the sample which remains stable within the potential range of -0.17 to 0.17 V. Beyond this potential range, the sample becomes susceptible to pitting. In the coated sample,

٢٥ the corrosion behavior is similar to that of the substrate, with the exception that the pseudo-

٢٦ passive layer remains stable within a narrower potential range of -0.19 to 0.08 V.

٢٧ *Keywords:* Electrodeposition, Ni–WC–TiC, Composite coating, Corrosion resistance

٢٨ ───────────────────────────

٢٩ *Corresponding author. Tel.: +98 (51) 3880-5106; Fax: +98 (51) 3880-7182.

٣٠ E-mail address: sayyedan@um.ac.ir (F.S. Sayyedan).

٣١   *1. Introduction*

٣٢   Surface protective coatings are highly in demand to improve corrosion resistance of materials by

٣٣   extending the life time of parts [1,2]. Employing composite structures in order to enrich the

٣٤   properties and performance of the coating has been of great interest in recent years [11,2-5]. The

٣٥   performance of the coatings can be improved by embedding reinforcing ceramic particles such as

٣٦   oxides (Al_2O_3), nitrides (TiN), carbides (WC, TiC), and intermetallic compounds (NiAl) within

٣٧   the composite matrix [2-5]. While the composite matrix could be Ni, Fe, Cu, Co, etc., nickel-based

٣٨   composite coatings are more in demand due to their desired mechanical properties and low cost

٣٩   [5,6]. Nickel coatings are widely used in petrochemical, textile [1], aerospace, piston rings,

٤٠   cylinders [3] and catalyst (Ni-CeO_2 composite) [7].

٤١   Corrosion is an aggressive phenomenon with economic and equipment losses which can be

٤٢   moderated employing composite coatings [2]. The observations have demonstrated that corrosion

٤٣   resistance of nickel composite coatings is better than that of the pure nickel coating, due to the

٤٤   formation of oxide layer and the presence of ceramic particles on the surface [8]. The corrosion

٤٥   properties of nickel-based coatings can be improved by adding tungsten to the matrix [3,8,9].

٤٦   Surender et al [4] investigated the corrosion resistance of electrodeposited Ni-WC composite

٤٧   coating. They realized that Ni-WC composite had higher current density and passive potential than

٤٨   that of the pure nickel. Adding TiN to the Ni-W composite by pulse electrodeposition method,

٤٩   Zhang et al [2] investigated the corrosion resistance of the composite coating and reported an

٥٠   improvement in the corrosion behavior of the composite coating in the presence of TiN.

٥١   While there are many methods to produce composites, one of the best processes could be the

٥٢   electrodeposition method [10,12]. Electrodeposition has been favored due to its ability to create

٥٣   complex shapes, low cost, reproducibility, and reduction of waste [1,10].

٥٤ The objective of this study was to investigate the effect of current density on the microstructure

٥٥ of electrodeposited (Ni-WC-TiC) composite coatings on AISI 304 stainless steel substrates,

٥٦ using micrometer-sized ceramic particles. After achieving optimal coating adhesion at the

٥٧ determined current density, the corrosion resistance of both the coating and substrate was

٥٨ evaluated in a 3.5 wt.% sodium chloride (NaCl) solution.

٥٩ *2. Materials and methods*

٦٠ AISI 304 stainless steel was cut into 2×2 cm^2 coupons. In order to connect an electric current, a

٦١ copper wire was connected to the pieces. The samples were mounted and grounded using 80 to

٦٢ 1200 SiC grit paper. The substrates were degreased in an ultrasonic bath subjected to acetone and

٦٣ distilled water for 20 minutes, respectively. Finally, the samples were subjected to pre-

٦٤ electrodeposition process according to the Table 1 in order to achieve better adhesion strength

٦٥ between the coating and the substrate.

٦٦ Table 1: The solutions used in the surface preparation stage for the next composite electroplating

Process No.	Solution	Time (s)	Details
1	6 ml distilled water + 4 ml HCl	50	Surface activation
2	30 ml distilled water + 70 ml H$_2$SO$_4$	180	Current density = 107 mA/cm^2 Anodic electrodeposition
3	120 ml HCl + 240 g/l NiCl	120	Current density = 108 mA/cm^2 Cathodic electrodeposition

٦٧

٦٨ In order to activate the surface of the substrate, the mounted coupons were immersed in the first

٦٩ solution. In the second solution, the piece was used as an anode, due to the detachment of atoms

٧٠ from the surface and roughening the substrate surface. The coupons were connected to the cathode

٧١ in the third solution to deposit NiCl on the 304 stainless steel surface. In the third stage, the carbide

٧٢ particles acquire a positive charge due to the applied electric field and migrate toward the cathode

٧٣ (substrate). Simultaneously, nickel ions undergo reduction by electron uptake and deposit onto the

٧٤ substrate, thereby entrapping the ceramic particles within the growing metallic matrix [29].

٧٥ Watts bath was prepared according to the Table 2 with a volume of 200 ml and let rest for 24 h. In

٧٦ order to prevent carbide particles to be settle, the prepared solution was placed in an ultrasonic

٧٧ bath for 15 min immediately before the start of the plating process. The carbide particles had a size

٧٨ of less than 25 μm, with a TiC/WC ratio of 1:2. The pH of the solution was adjusted by NH_3 and

٧٩ 98 vol.% diluted sulfuric acid using a digital PH meter (Metrohm, Switzerland) within the

٨٠ specified range. Electrodeposition process was run by direct current method and digital coulometer

٨١ device (Behpajooh, Iran) under a temperature of 50°C and conditions presented in Table 3. The

٨٢ samples were rinsed with ethanol after the coating process. In this research, electrodeposition was

٨٣ run under four different current densities of 30, 35, 40, and 50 mA/cm^2. Fig. 1 depicts an overview

٨٤ of the Watts solution along with the presence of WC and TiC particles for the coating process.

٨٥ Table 2: Watts bath composition for nickel electrodeposition

Composition	Concentration (g/l)	Company
$NiCl_2.6H_2O$	45	MERCK
H_3BO_3	40	MERCK
TiC-WC	6	MERCK
$NiSO_4$	250	MERCK

٨٦

٨٧ Table 3: Nickel electrodeposition conditions

Current	DC
Temperature (°C)	50±2
pH	4.4±0.1
Colon (A.S)	27
Anode	Nickel
Cathode	AISI 304 stainless steel

٨٨

٨٩

٩٠

٩١

٩٢
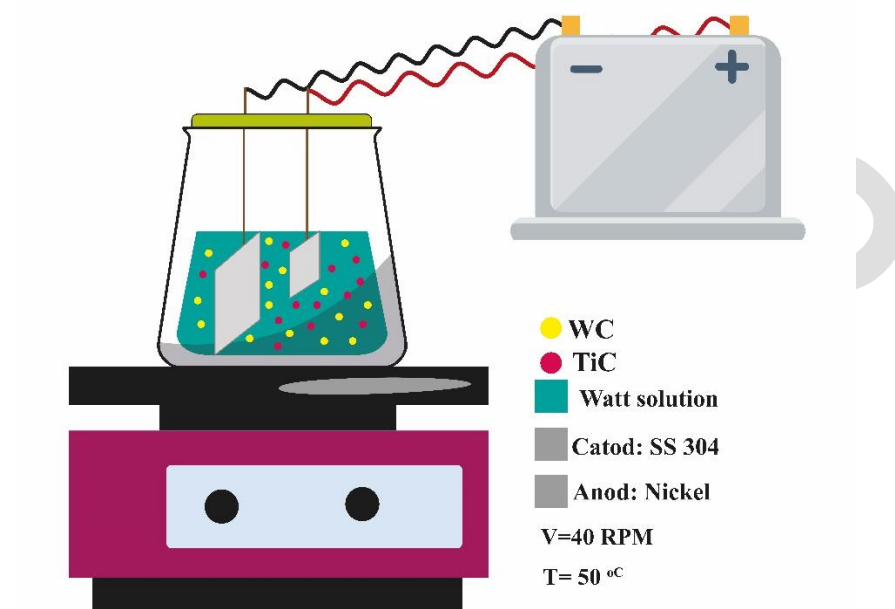
٩٣   Fig. 1: Schematic of the Watts solution used in the coating process

٩٤ The surface morphology of the coatings was observed using a scanning electron microscope (SEM,

٩٥ Philips XL30). The elemental composition of the produced composite was analyzed by the energy

٩٦ dispersive spectroscopy (EDS). The phase composition of the coatings was investigated by X-ray

٩٧ diffraction (XRD) method (40 Kv, Cu K_α). Phase analysis was performed using X'Pert HighScore

٩٨ software. The crystallite size (d) of the coating was determined using the Scherer equation (Eq. 1).

٩٩ $d = K\lambda/\beta.\cos\theta$ (1)

١٠٠   Where, k is the Scherer's constant with the value of 0.91, λ is the wavelength of the beam used

١٠١   (1.542 Å for copper), β is the peak width at half-height (FHWM), and θ is the Bragg diffraction

١٠٢   angle.

١٠٣   Electrochemistry Impedance spectroscopy (EIS) and Potantiodynamic polarization tests were

١٠٤   performed in 3.5 wt.% NaCl solution to examine the corrosion behavior of the coated and uncoated

١٠٥   samples.

١٠٦   The three-electrode electrochemical cell, consisting of the sample as the working electrode, a KCl

١٠٧   saturated Ag/AgCl electrode as the reference electrode, and a platinum electrode as the counter

١٠٨   electrode, was connected to the potentiostat device (Ivium, Netherlands). After immersing the

١٠٩   sample in a 3.5 wt.% NaCl electrolyte for one hour, the Electrochemical Impedance Spectroscopy

١١٠   (EIS) test was conducted within the frequency range of 100 kHz to 10 mHz at a voltage amplitude

١١١   of 10 mV followed by the dynamic polarization test in the potential range from -250 mV relative

١١٢   to the open-circuit potential (OCP) to 1.6 V relative to the reference electrode. The surface

١١٣   morphology of the samples after corrosion test in salt environment was observed by scanning

١١٤   electron microscope (SEM, Philips XL30).

١١٥   *3. Results and discussion*

١١٦   The SEM micrographs of the coatings with current densities of 30, 35, 40, and 50 mA/cm^2 and

١١٧   carbide concentration of 6 g/l are presented in Fig. 2. It can be seen that a uniform and dense

١١٨   coating could be achieved by increasing the current density up to 40 mA/cm^2. Further increase in

١١٩   current density up to 50 mA/cm^2 caused a decrease in the uniformity and density of the coating

١٢٠   with some scattered carbide particles deposited in the matrix. It is known that for a constant carbide

١٢١   concentration, the growth rate of the nuclei remains almost the same with the reduction of the

١٢٢   current density, and a more uniform morphology would be obtained [13]. At lower current

١٢٣ densities the deposits on the cathode surface are limited [14,15]. At the optimal current density (40

١٢٤ mA/cm^2), the growth of nickel is sufficient to trap deposits in a certain period of time leading to

١٢٥ an increase in deposition. On the other hand, the rate of carbide deposition increases with

١٢٦ increasing the current density followed by an increase in the growth rate of the coating and the

١٢٧ amount of carbide deposited [14,16,17]. Therefore, it will be possible to choose the optimal limit

١٢٨ of the current density to achieve a uniform and dense coating, based on the observations of surface
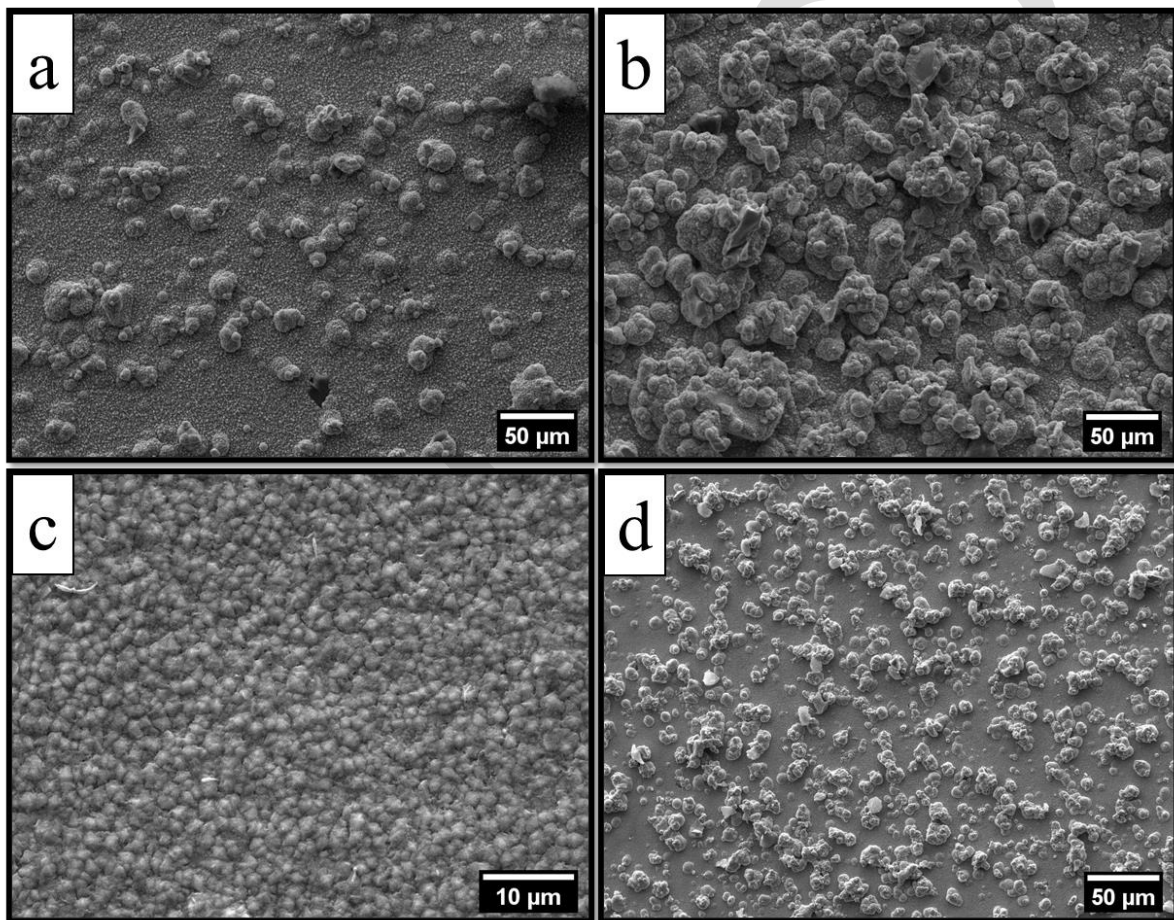
١٢٩ morphology and elemental analysis.

١٣٠

١٣١ Fig. 2: SEM micrographs of Ni–WC–TiC composite coating surface at different current densities:

١٣٢ a) 30 mA/cm^2, b) 35 mA/cm^2, c) 40 mA/cm^2, d) 50 mA/cm^2

١٣٣ Fig. 3 represents the EDS analysis of the coating at different current densities. Accordingly, as the

١٣٤ current density increases, the percentage of carbide deposition increases, which can be explained

١٣٥ by the Faraday's first law (Eq. 2) [17]:

١٣٦ $m = Kq = KIt$ (2)

١٣٧ Where, m is the mass deposited, I is the electrical current, t is the electrolysis time, q is the total

١٣٨ charge, and K is the equivalent weight of the electrolyte. The equivalent weight is expressed as

١٣٩ atomic weight divided by valency. According to equation (2), m is proportional to I. It means that

١٤٠ the higher the current density, the more ions carrying the composite agent in the solution followed

١٤١ by an increase in the deposited mass. The results of the EDS analysis of the coating at different

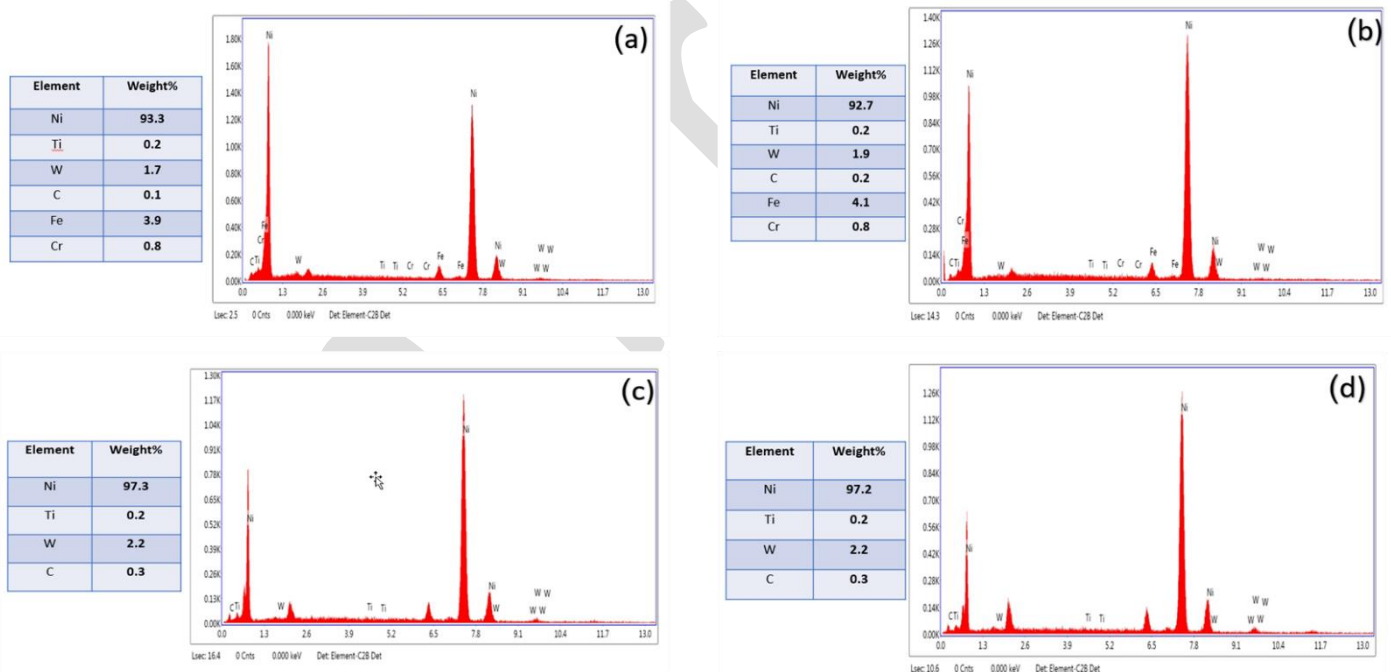١٤٢ current densities also confirmed this fact (Fig. 3).

١٤٣ Fig. 3: EDS analysis of Ni–WC–TiC composite coating at different current densities: a) 30 mA/cm^2,

١٤٤ b) 35 mA/cm^2, c) 40 mA/cm^2, and d) 50 mA/cm^2

١٤٥ According to the SEM images and EDS analysis of the coating in different current densities, the

١٤٦ current density of 40 mA/cm^2 was obtained to be the optimal current density in which a uniform

١٤٧   and dense coating with desired amount of double carbide deposition would been obtained. In the

١٤٨   next section, the results of the XRD analysis and corrosion resistance of the coating will be

١٤٩   discussed at the optimal current density of 40 mA/cm^2.

١٥٠   Fig.4 illustrates the cross-sectional morphology of the coating at a current density of 40 mA/cm².

١٥١   As observed, the coating is densely packed and fully adhered to the substrate surface, with a

١٥٢   thickness raging from 10 to 37 µm. However, at greater coating thicknesses, the uniformity

١٥٣   diminishes, and the coating tends to accumulate in localized areas. This discontinuity and non-

١٥٤   uniformity could also be attributed to the cutting process performed on the sample to observe the

١٥٥   cross-section. On average, the coating thickness was measured to be 24±0.8 µm. The dark areas

١٥٦   in Fig. 3 represent nickel particles serving as the matrix, while the white areas indicate undissolved

١٥٧   WC particles within the composite matrix. The WC particles have retained their structure and

١٥٨   accumulated at the end of the coating. Due to the addition of Ti to the coating, the number of these

١٥٩   particles is not significant. Ti facilitates the dissolution of WC particles in the coating [18].
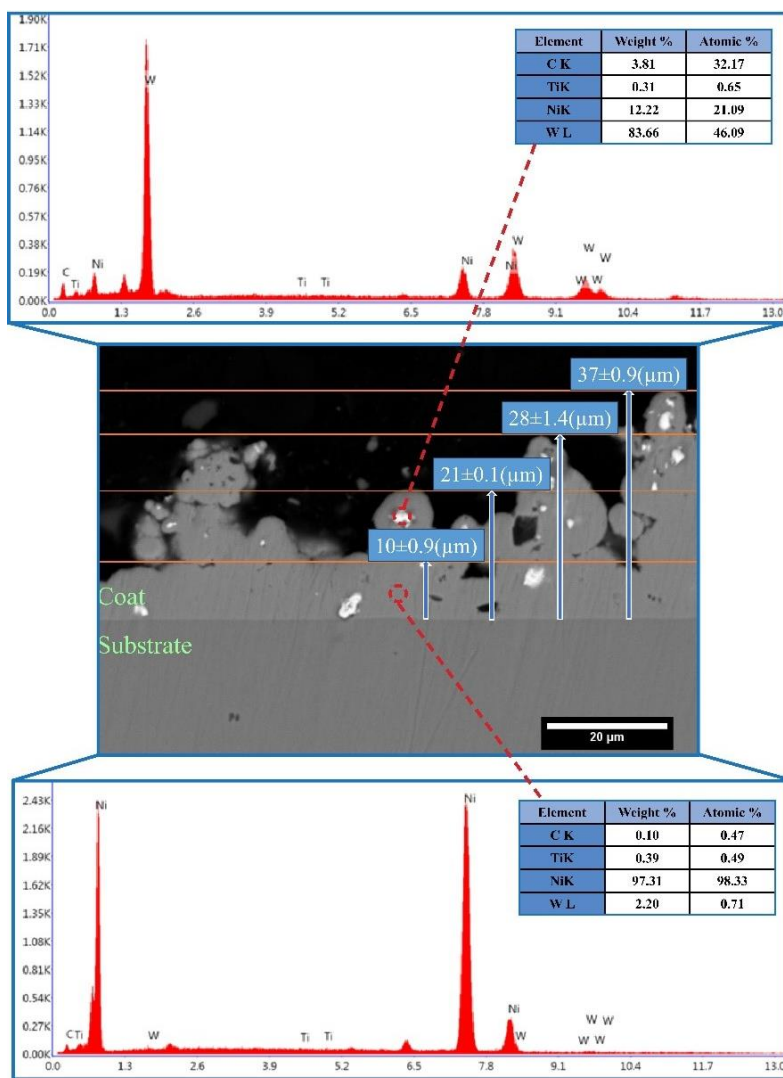
١٦٠

١٦١   Fig. 4: SE-SEM image of the cross section of the Ni–WC–TiC composite coating at the current density

١٦٢   of 40 mA/cm^2

١٦٣   The XRD analysis of the coating at the current density of 40 mA/cm^2 is presented in Fig. 5. The

١٦٤   obtained diffraction patterns indicated the presence of the Ni phase with a cubic crystal structure

١٦٥   and ceramic hard phases of WC-TiC in the composite coating. X'pert High Score software

١٦٦   calculates the crystallite size using equation 1. The calculated crystallite size for the index peak

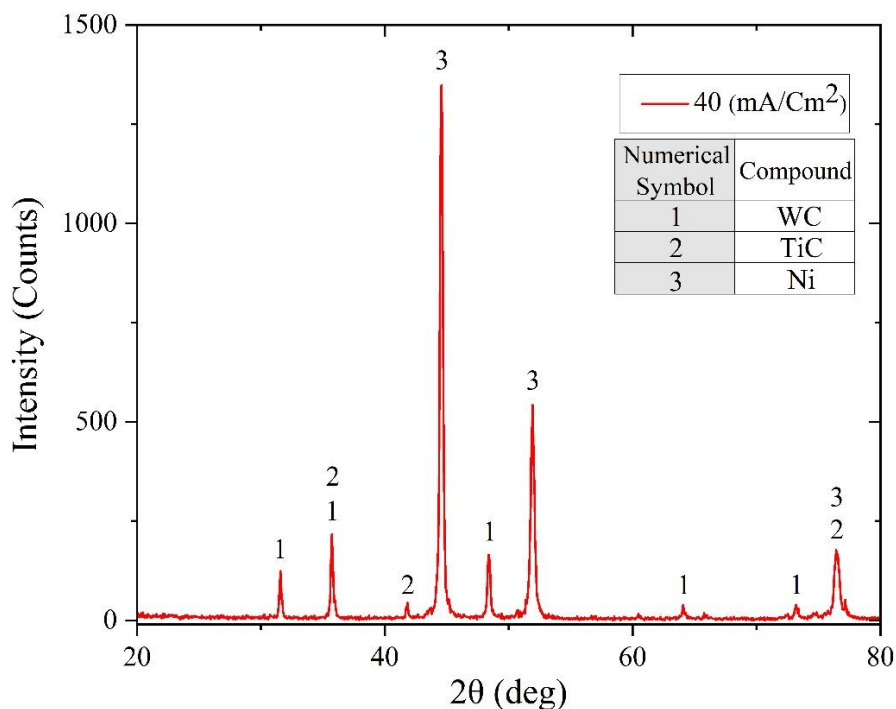١٦٧   according to the Scherer equation was obtained to be 390 Å.

١٦٩   Fig. 5: XRD analysis of the Ni–WC–TiC composite coating at the current density of 40 mA/cm^2

١٧٠   The EIS test plots are presented in Fig. 6, including Nyquist, Term, and Bode phase diagrams. The

١٧١   data extracted from the ZView software are summarized in Table 4 and the equivalent circuit

١٧٢   corresponding to the impedance curves is shown in Fig. 7. In the Nyquist plot, a larger loop radius

١٧٣   indicates higher resistance of the sample [27]. According to the Fig. 6a, the substrate exhibits

١٧٤   greater resistance compared to the coated sample. Additionally, the Term and Bode phase plots

١٧٥   reveal the presence of three time constants, indicating three loops in the equivalent circuit predicted

١٧٦   by ZView software. The presence of three distinct regions with varying slopes and concavities

١٧٧   suggests the existence of three time constants and, consequently, three loops in the equivalent

١٧٨   circuit. The three-loop configuration of the equivalent circuit can be attributed to the corrosion

١٧٩   phenomenon, which introduces three time constants: R_S, representing the solution resistance; R_1,

١٨٠ representing the resistance of the passive layer; R_2, corresponding to the charge transfer resistance

١٨١ of the steel sample's dissolution process within pits; and R_3, representing charge transfer resistance.

١٨٢ A constant phase element (CPE) is also employed to account for the non-ideal capacitance due to

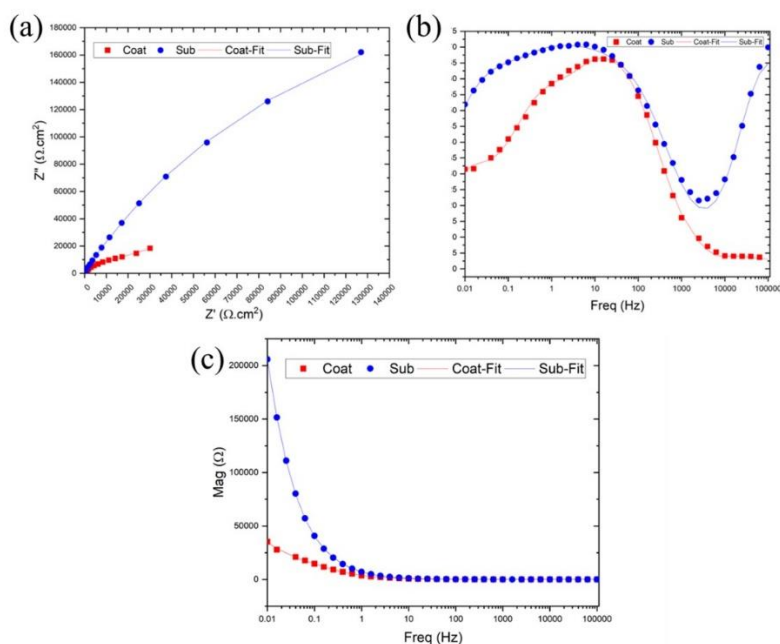١٨٣ the deviation of the semicircle from a perfect circular shape

١٨٤ [26].

١٨٥

١٨٦ Fig.6. The curves obtained from the impedance test: (a) Nyquist, (b) Term phase, and (c) Bode phase
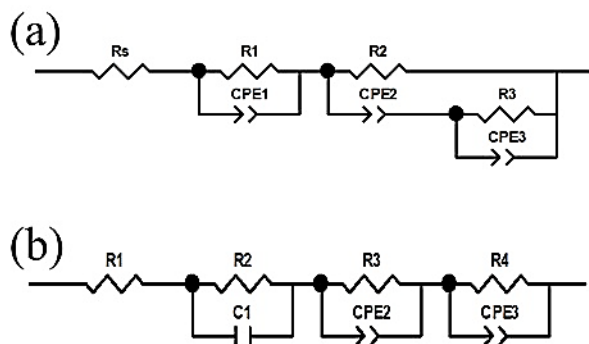

١٨٧

١٨٨ Fig.7. The equivalent circuit predicted by the ZView software including the equivalent circuit of (a) the

١٨٩ coating (b) the substrate

۱۹۰   The impedance of CPE is defined as below [20]:

۱۹۱     $Z_{CPE} = \dfrac{1}{Q(\omega.i)^{-n}}$ (3)

۱۹۲   Where, Q and n (between 0-1) are constants of CPE, ω is angular frequency, and I is imaginary

۱۹۳   number ($i^2=1$).

۱۹٤   As can be observed from the plots and the results presented in Table 4, the substrate sample

۱۹٥   exhibits higher corrosion resistance compared to the coated one.

۱۹٦   Table 4: The parameters extracted from the impedance test results by Z-View software

Parameter	Substrate	Coating
$R_S(\Omega.cm^2)$	20	46.57
$R_1 (\Omega.cm^2)$	2077	581.7
$Q_1(F/ cm^2)$	-	10.8×10^{-5}
n_1	-	0.91
$R_2(\Omega.cm^2)$	47.86	63370
$Q_2(F/ cm^2)$	2.2×10^{-7}	20.1×10^{-5}
n_2	0.96	0.83
$R_3(\Omega.cm^2)$	600480	17556
$Q_3(F/ cm^2)$	0.36×10^{-4}	8.6×10^{-5}
n_3	0.78	0.81
$C_1(F/ cm^2)$	308.8×10^{-6}	-
Chi-squared	0.0013	0.0003

۱۹۷   The results of the potantiodynamic polarization test in 3.5 wt.% NaCl solution for the coated and

۱۹۸   uncoated samples are presented in Fig. 8. The results extracted from the polarization plots (Fig. 8)

۱۹۹   are presented in Table 5, where "E_b" and "E_{corr}" represent the breakdown potential of the passive

۲۰۰   layer and the corrosion potential of the samples, respectively.

۲۰۱   Based on the dynamic polarization test plots, the corrosion mechanism of the substrate is active-

۲۰۲   quasi passive, with a pseudo-passive layer forming on the sample which remains stable within the

۲۰۳   potential range of -0.17 to 0.17 V. Beyond this potential range, the sample becomes susceptible to

٢٠٤   pitting. In the coated sample, the corrosion behavior is similar to that of the substrate, with the

٢٠٥   exception that the pseudo-passive layer remains stable within a narrower potential range of

٢٠٦   -0.19 to 0.08 V.

٢٠٧
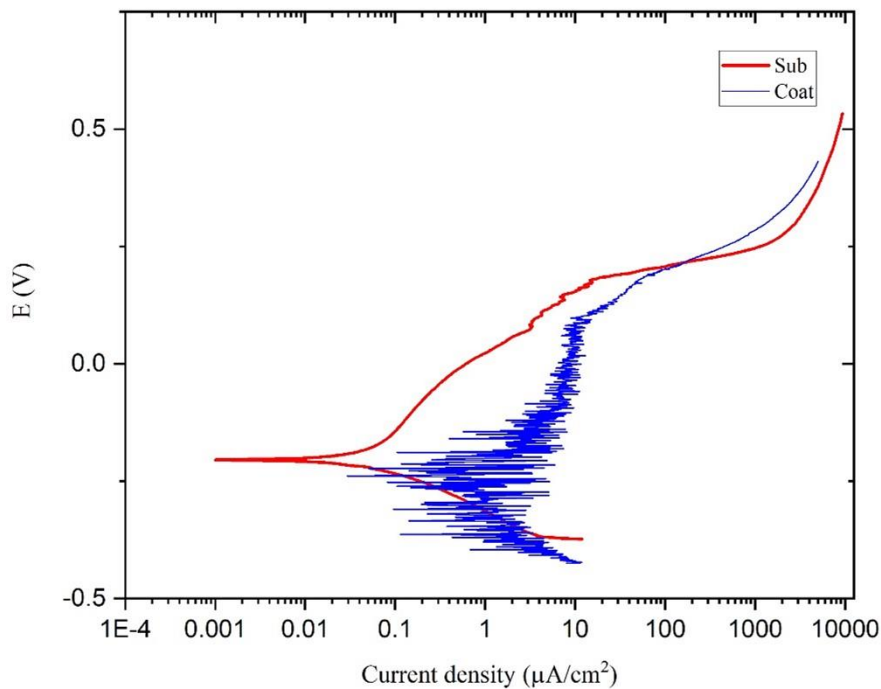
٢٠٨   Fig. 8: Polarization test of the coated and uncoated samples in 3.5 wt.% NaCl solution

٢٠٩   Table 5: The results of the polarization test for the substrate and coating

Sample	E_{corr}(v)	E_b
Substrate	-0.22	0.17
Composite coating	-0.29	0.08

٢١٠   According to the corrosion theories, the corrosion intensity depends on the number and size of

٢١١   holes and defects present in the coating. The holes in the coating cause the formation of micro

٢١٢   galvanic cells by transferring the electrolyte from the environment to the coating/substrate

٢١٣   interface leading to an increase in the corrosion rate [19]. Also, coating defects such as porosity,

٢١٤   coating layer thickness, and microcracks affect the corrosion resistance. These defects cause

٢١٥   chloride ions to reach the substrate and increase susceptibility to pitting corrosion [21,28].

٢١٦   Fig. 9. presents the SEM images of the surface of the coated sample at the current density of 40

٢١٧   mA/cm^2 after corrosion in 3.5 wt.% NaCl solution with two different magnifications. The

٢١٨   composite coating owns some small and large holes responsible for chloride ions transport to the

٢١٩   surface of the substrate and cause pitting corrosion and galvanic corrosion of the coating and the

٢٢٠   substrate. Another reason for pitting and galvanic corrosion is the presence of nickel. The corrosion

٢٢١   mechanism of Ni coating is mainly pitting and galvanic corrosion [22]. Xia et al [23] reported that

٢٢٢   small-sized ceramic particles can significantly increase the corrosion resistance and stability of the

٢٢٣   metal-matrix composites. So, the small particles of TiC and WC in the Ni matrix can provide the

٢٢٤   best corrosion resistance for the coating. As a result, with the presence of WC particles in the

٢٢٥   composite coating, Ni matrix is less exposed to corrosion and the corrosion resistance of the

٢٢٦   coating increases. This effect is also observed in the presence of grain boundaries that have low

٢٢٧   corrosion resistance. So, the corrosion resistance of the coating increases in the presence of WC in

٢٢٨   the grain boundaries [22,24,25]. Fig. 9, reveals that due to the creation of macro and micro particles

٢٢٩   and the creation of small and large holes during deposition of the coating, the homogeneous

٢٣٠   structure of the coating has been partially destroyed leading to the transfer of electrolyte from

٢٣١   small defects to the substrate. This issue causes a small change in the corrosion resistance of the

٢٣٢   substrate. Not much change in the corrosion resistance of the coating compared to the substrate is

٢٣٣   due to the non-uniform distribution of WC and TiC carbide particles in the nickel matrix. Another

٢٣٤   reason could be the low amount of WC and TiC carbides in the Watts bath solution. In this case,

٢٣٥   the pitting corrosion mechanism in nickel (the main corrosion mechanism) is activated and the

٢٣٦   corrosion phenomenon starts for the coating. But, in the case of a more uniform distribution of

٢٣٧   carbide particles or a larger number of carbides, the corrosion resistance increases as the presence

٢٣٨   of the carbide particles increases the corrosion resistance of the coating.
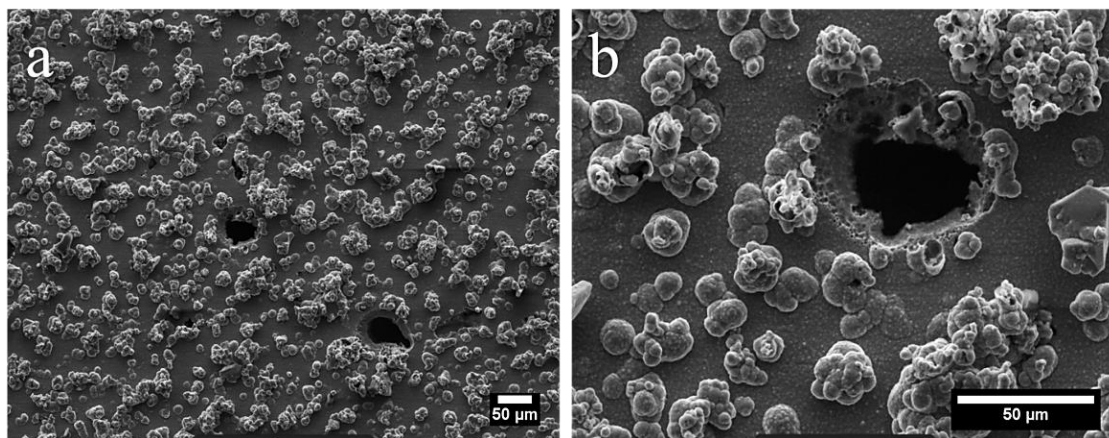
٢٣٩

٢٤٠   Fig. 9: SEM images of the surface of the coated sample with a current density of 40 mA/cm^2 after

٢٤١   corrosion in 3.5 wt.% NaCl solution with two different magnifications

٢٤٢   *4. Conclusions*

٢٤٣   In this research, Ni–WC–TiC composite coating was applied on the AISI 304 stainless steel by the

٢٤٤   electrodeposition method and the effect of current density on the coating microstructure was

٢٤٥   investigated at the constant carbide concentration of 6 g/l. The results of the SEM/EDS

٢٤٦   observations revealed that the optimal current density to achieve a denser microstructure with more

٢٤٧   continuity and uniformity compared to others was 40 mA/cm^2. The impedance and polarization

٢٤٨   tests of the substrate and coating revealed the greater resistance of the substrate compared to the

٢٤٩   coating, as well as the quasi-passive behavior of the samples in the polarization test.

٢٥٠

٢٥١

٢٥٢

٢٥٣

٢٥٤

٢٥٥

٢٥٦ *References*

٢٥٧
٢٥٨
٢٥٩
1. S. Khorsand, M. Karbasi, F. S. Sayyedan, M. Eshaghian, and M. Razavi, Development of electroco-deposited Ni–Fe(Ti,W)C nanocomposite coatings, Surf. Eng. 34 (2018) 433–439. doi:10.1080/02670844.2017.1370880.

٢٦٠
٢٦١
٢٦٢
2. W. Zhang, B. Li, and C. Ji, Synthesis and characterization of Ni-W/TiN nanocomposite coating with enhanced wear and corrosion resistance deposited by pulse electrodeposition, Ceram. Int. 45 (2019) 14015–14028. doi: 10.1016/j.ceramint.2019.04.101.

٢٦٣
٢٦٤
٢٦٥
٢٦٦
3. N. P. Wasekar, L. Bathini, L. Ramakrishna, D. S. Rao, and G. Padmanabham, Pulsed electrodeposition, mechanical properties and wear mechanism in Ni-W/SiC nanocomposite coatings used for automotive applications, Appl. Surf. Sci. 527 (2020) 146896. doi: 10.1016/j.apsusc.2020.146896.

٢٦٧
٢٦٨
٢٦٩
4. M. Surender, R. Balasubramaniam, and B. Basu, Electrochemical behavior of electrodeposited Ni–WC composite coatings, Surf. Coatings Technol. 187 (2004) 93–97. doi: 10.1016/j.surfcoat.2004.01.030.

٢٧٠
٢٧١
٢٧٢
5. M. Qunshuang, L. Yajiang, and W. Juan, Effects of Ti addition on microstructure homogenization and wear resistance of wide-band laser clad Ni60/WC composite coatings, Int. J. Refract. Met. Hard Mater. 64 (2017) 225–233. doi: 10.1016/j.ijrmhm.2016.11.002.

٢٧٣
٢٧٤
٢٧٥
٢٧٦
6. M. Bedolla-Hernández, G. Rosano-Ortega, F. J. Sánchez-Ruiz, J. Bedolla-Hernández, P. S. Schabes-Retchkiman, and C. A. Vega-Lebrún, Electrodeposition mechanism of chromium nanoparticle coatings: Modeling and experimental validation, Chem. Eng. Sci. 252 (2022) 117291. doi: 10.1016/j.ces.2021.117291.

٢٧٧
٢٧٨
٢٧٩
7. H. Hasannejad and T. Shahrabi, Economical deposition of Ni high cerium oxide nanocomposite coatings, Surf. Eng. 28 (2012) 418–423. doi: 10.1179/1743294411Y.0000000086.

٢٨٠
٢٨١
٢٨٢
٢٨٣
8. Z. Zhang et al., Electrodeposition and wear behavior of NiCoW ternary alloy coatings reinforced by Al2O3 nanoparticles: Influence of current density and electrolyte composition, Surf. Coatings Technol. 431 (2022) 128030. doi: 10.1016/j.surfcoat.2021.128030.

٢٨٤
٢٨٥
٢٨٦
9. A. Chianpairot, G. Lothongkum, C. A. Schuh, and Y. Boonyongmaneerat, Corrosion of nanocrystalline Ni–W alloys in alkaline and acidic 3.5wt.% NaCl solutions, Corros. Sci. 53 (2011) 1066–1071. doi: 10.1016/j.corsci.2010.12.001.

٢٨٧
٢٨٨
٢٨٩
10. D. K. Singh and V. B. Singh, Electrodeposition and characterization of Ni–TiC composite using N-methylformamide bath, Mater. Sci. Eng. 532 (2012) 493–499. doi: 10.1016/j.msea.2011.10.115.

٢٩٠
٢٩١
٢٩٢
11. S. A. Lajevardi and T. Shahrabi, Effects of pulse electrodeposition parameters on the properties of Ni–TiO2 nanocomposite coatings, Appl. Surf. Sci. 256 (2010) 6775–6781. doi: 10.1016/j.apsusc.2010.04.088.

٢٩٣ 12. A. Bigos et al., Citrate-based baths for electrodeposition of nanocrystalline nickel coatings
٢٩٤   with enhanced hardness, J. Alloys Compd. 850 (2021) 156857. doi:
٢٩٥   10.1016/j.jallcom.2020.156857.

٢٩٦ 13. F. Ebrahimi and Z. Ahmed, The effect of current density on properties of electrodeposited
٢٩٧   nanocrystalline nickel. J. Appl. Electrochem. 33 (2003) 733–739. doi:
٢٩٨   10.1023/A:1025049802635.

٢٩٩ 14. P. Gyftou, M. Stroumbouli, E. A. Pavlatou, and N. Spyrellis, Electrodeposition of Ni/SiC
٣٠٠   Composites by Pulse Electrolysis, Trans. IMF. 80 (2002) 88–91. doi:
٣٠١   10.1080/00202967.2002.11871440.

٣٠٢ 15. J. L. Stojak and J. B. Talbot, Investigation of Electrocodeposition Using a Rotating
٣٠٣   Cylinder Electrode, J. Electrochem. Soc. 146 (1999) 4504–4513. doi: 10.1149/1.1392665.

٣٠٤ 16. Y. Xuetao, W. Yu, S. Dongbai, and Y. Hongying, Influence of pulse parameters on the
٣٠٥   microstructure and microhardness of nickel electrodeposits, Surf. Coatings Technol. 202
٣٠٦   (2008) 1895–1903. doi: 10.1016/j.surfcoat.2007.08.023.

٣٠٧ 17. M. E. Gamboa-Adelco and R. J. Gale, A Guide to Problems in Modern Electrochemistry
٣٠٨   1. Boston, MA: Springer US, 2001. doi: 10.1007/978-1-4419-8600-9.

٣٠٩ 18. L. Venkatesh et al., Microstructure and phase evolution in laser clad chromium carbide-
٣١٠   NiCrMoNb, Appl. Surf. Sci. 357 (2015) 2391–2401. doi: 10.1016/j.apsusc.2015.09.260.

٣١١ 19. S. Kamkar, M. Mohammadi and M. Karimi, Assessment of the Corrosion and Tribological
٣١٢   Properties of Double Layer Nitride Coatings Performed by Plasma Nitriding and Cathodic
٣١٣   Arc Evaporation on Ti-6Al-4V Alloy, 20 (2020) 1555–1565.

٣١٤ 20. L. Zhang, X. Tang, Z. Wang, T. Li, Z. Zhang, and M. Lu, The Corrosion Behavior of 316L
٣١٥   Stainless Steel in H2S environment at high temperatures, Int. J. Electrochem. Sci. 12
٣١٦   (2017) 8806–8819. doi: 10.20964/2017.09.17.

٣١٧ 21. A. Günen, B. Soylu, and Ö. Karakaş, Titanium carbide coating to improve surface
٣١٨   characteristic, wear and corrosion resistance of spheroidal graphite cast irons, Surf.
٣١٩   Coatings Technol. 437 (2022) 128280. doi: 10.1016/j.surfcoat.2022.128280.

٣٢٠ 22. X. Yang, X. Li, Q. Yang, H. Wei, X. Fu, and W. Li, Effects of WC on microstructure and
٣٢١   corrosion resistance of directional structure Ni60 coatings, Surf. Coatings Technol. 385
٣٢٢   (2020) 125359. doi: 10.1016/j.surfcoat.2020.125359.

٣٢٣ 23. F. F. Xia, W. C. Jia, C. Y. Ma, R. Yang, Y. Wang, and M. Potts, Synthesis and
٣٢٤   characterization of Ni-doped TiN thin films deposited by jet electrodeposition, Appl. Surf.
٣٢٥   Sci.434 (2018) 228–233. doi: 10.1016/j.apsusc.2017.10.203.

٣٢٦ 24. N. Dai, L. C. Zhang, J. Zhang, Q. Chen, and M. Wu, Corrosion behavior of selective laser
٣٢٧   melted Ti-6Al-4 V alloy in NaCl solution, Corros. Sci. 102 (2016) 484–489. doi:
٣٢٨   10.1016/j.corsci.2015.10.041.

٣٢٩ 25. J. D. Voorhies, Electrochemical and Chemical Corrosion of Tungsten Carbide (WC), J.
٣٣٠   Electrochem. Soc. 119 (1972) 219. doi: 10.1149/1.2404164.

٣٣١ 26. W. Wang, L. Qian, Y. Zhang, and Y. Zhang, Electrochemical impedance spectroscopy
٣٣٢   characteristics of steel corrosion in seawater sea-sand concrete, IOP Conf. Ser. Earth
٣٣٣   Environ. Sci. 267 (2019) 042017. doi: 10.1088/1755-1315/267/4/042017.

٣٣٤ 27. M. Saremi and M. Yeganeh, Corrosion behavior of copper thin films deposited by EB-
٣٣٥   PVD technique on thermally grown silicon dioxide and glass in hydrochloric acid media,
٣٣٦   Mater. Chem. Phys. 123 (2010) 456–462. doi: 10.1016/j.matchemphys.2010.04.041.

٣٣٧ 28. S.A. Naziri Mehrabani, R. Ahmadzadeh, N. Abdian, A. Taghizadeh Tabrizi, and H.
٣٣٨   Aghajani, Synthesis of Ni-GO nanocomposite coatings: Corrosion evaluation, Surf.
٣٣٩   Interfaces. 20 (2020) 100546. doi.org/10.1016/j.surfin.2020.100546.

٣٤٠ 29. N. Guglielmi, Kinetics of the Deposition of Inert Particles from Electrolytic Baths, J.
٣٤١   Electrochem. Soc. 119 (1972) 1009-1012. **doi** 10.1149/1.2404383.